Calcium-axonemal microtubuli interactions underlie mechanism(s) of primary cilia morphological changes.

Buljan VA, Graeber MB; Vuletić, Vladimira

Download date / Datum preuzimanja: **2024-09-01**

CrossMark

ORIGINAL PAPER

Calcium–axonemal microtubuli interactions underlie mechanism(s) of primary cilia morphological changes

Vlado A. Buljan[1,2] · **Manuel B. Graeber**[1,2] ·
R. M. Damian Holsinger[3,4] · **Daniel Brown**[1] ·
Brett D. Hambly[5] · **Edward J. Delikatny**[6] ·
Vladimira R. Vuletic[7] · **Xavier N. Krebs**[1] ·
Ilijan B. Tomas[8] · **John J. Bohorquez-Florez**[1] ·
Guo Jun Liu[9] · **Richard B. Banati**[1,3,9],

Abstract We have used cell culture of astrocytes aligned within microchannels to investigate calcium effects on primary cilia morphology. In the absence of calcium and in the presence of flow of media (10 $\mu L.s^{-1}$) the majority (90%) of primary cilia showed reversible bending with an average curvature of $2.1 \pm 0.9 \times 10^{-4}$ nm^{-1}. When 1.0 mM calcium was present, 90% of cilia underwent bending. Forty percent of these cilia demonstrated strong irreversible bending, resulting in a final average curvature of $3.9 \pm 1 \times 10^{-4}$ nm^{-1}, while 50% of cilia underwent bending similar to that observed during calcium-free flow. The average length of cilia was

✉ Vlado A. Buljan
  vlado.buljan@sydney.edu.au

✉ Manuel B. Graeber
  manuel.graeber@sydney.edu.au

  R. M. Damian Holsinger
  damian.holsinger@sydney.edu.au

  Daniel Brown
  daniel.brown@sydney.edu.au

  Brett D. Hambly
  brett.hambly@sydney.edu.au

  Edward J. Delikatny
  delikatny@rad.upenn.edu

  Vladimira R. Vuletic
  vladimira.vuletic@kbc-rijeka.hr

  Xavier N. Krebs
  xavier.krebs@gmail.com

Springer

shifted toward shorter values (3.67 ± 0.34 μm) when exposed to excess calcium (1.0 mM), compared to media devoid of calcium (3.96 ± 0.26 μm). The number of primary cilia that became curved after calcium application was reduced when the cell culture was pre-incubated with 15 μM of the microtubule stabilizer, taxol, for 60 min prior to calcium application. Calcium caused single microtubules to curve at a concentration ≈ 1.0 mM in vitro, but at higher concentration (≈ 1.5 mM) multiple microtubule curving occurred. Additionally, calcium causes microtubule-associated protein-2 conformational changes and its dislocation from the microtubule wall at the location of microtubule curvature. A very small amount of calcium, that is 1.45×10^{11} times lower than the maximal capacity of TRPPs calcium channels, may cause gross morphological changes (curving) of primary cilia, while global cytosol calcium levels are expected to remain unchanged. These findings reflect the non-linear manner in which primary cilia may respond to calcium signaling, which in turn may influence the course of development of ciliopathies and cancer.

Keywords Primary cilia · Calcium · Axonemal microtubules · Interactions · Morphology · Nonlinear dynamics

Ilijan B. Tomas
tomas.ilijan@kbo.hr

John J. Bohorquez-Florez
jboflo@yahoo.com.au

Guo Jun Liu
guojun.liu@ansto.gov.au

Richard B. Banati
richard.banati@sydney.edu.au

[1]   Brain Tumor Research Laboratories, Brain and Mind Center, Sydney Medical School and Faculty of Health Sciences, University of Sydney, Sydney, NSW 2050, Australia

[2]   Discipline of Anatomy and Embryology, School of Medical Sciences, Sydney Medical School, Charles Perkins Centre and Bosch Institute, University of Sydney, Sydney, NSW 2006, Australia

[3]   Laboratory of Molecular Neuroscience and Dementia, Brain and Mind Center, Sydney Medical School, University of Sydney, Sydney, NSW 2050, Australia

[4]   Discipline of Biomedical Science, School of Medical Sciences, Sydney Medical School, University of Sydney, Lidcombe, NSW 1825, Australia

[5]   Discipline of Pathology, School of Medical Sciences, Sydney Medical School, Bosch Institute, University of Sydney, Sydney, NSW 2006, Australia

[6]   Department of Radiology, University of Pennsylvania, Philadelphia, PA 19104, USA

[7]   Clinical Department of Neurology, UHC Rijeka, Medical Faculty Rijeka, Rijeka, Croatia

[8]   Department of Oncology and Radiotherapy, Medical Faculty, University 'Josip Juraj Strossmayer', 31000 Osijek, Croatia

[9]   Australian Nuclear Sciences and Technology Organisation (ANSTO), The Bragg Institute and the Australian Synchrotron, Sydney, Australia

1 Introduction

1.1 General considerations

Primary cilia are solitary, non-motile, typically slender and cylindrical cellular membrane protuberances (Fig. 1a, b) as discussed in a number of papers [1–3].

It is due to the numerous membrane receptors, channels, and also primary cilia's skeleton (constituted of nine radially arranged doublets of microtubules, known as the axonemal microtubules) that primary cilia are considered cellular sensory sub-systems that are critically important in both health and disease [4, 5]. Primary cilia are found during interphase in almost all eukaryotic cells, while during other cellular stages they appear to be reabsorbed [6].

In this study, the interaction between calcium/microtubules has been studied to examine the sensing aspect of the informational system of primary cilia, which is illustrated schematically in Fig. 1c. Briefly, this informational system begins with calcium-based channels (known as polycystin 1/2 (TRPP1/2)) located at the primary cilia membrane. Once detected, this system picks up extracellular environmental signals, expressed as calcium changes. The signal is further processed by primary cilia axonemal microtubules' doublets and subsequently by triplets of centriole microtubules positioned in the pericentrosomal matrix. Finally, the signal is transduced deep into the intracellular space, where it can be transduced and integrated within intracellular signaling cascades, influencing important ongoing intracellular processes, such as the cell cycle [7–9].

Importantly, the primary cilium is a dynamic structure that can disassemble and reassemble in conjunction with specific environmental changes. This includes rapid and reversible morphological changes, from slight changes in length and curvature to complete disappearance and reappearance, in response to different biophysical-biochemical environmental conditions [10–17]. These changes are enabled by modifications of the primary cilium skeleton, for example, in axonemal microtubules [18]. The very direct role of primary cilium axonemal microtubules in defining its morphology in response to changes of environmental conditions is demonstrated in microfluidic experiments that have shown how primary cilia respond to tightening of the space of their physical confinement by shortening their length [19, 20].

Morphological changes within the primary cilium, such as change of length or bending, may directly interfere with the function of the calcium signaling mechanism of primary cilia receptors and channels. Therefore, it is likely that, due to these specific morphological changes, as a specific response to environmental conditions, primary cilia have a particularly critical role in tissue morphogenesis and homeostasis, indicating their potential role in carcinogenesis [15, 21–26]. Indeed, primary cilia may assume a pathological appearance, become reduced in number, or become completely lost in different cancers, as shown in astrocytoma/glioblastoma cell lines, the pre-invasive and invasive stages of prostate cancer, and in breast cancer [5, 15, 27–29].

Furthermore, structurally aberrant primary cilia or their complete absence may lead to incomplete integration of signal transduction and, consequently, to disastrous illnesses known as ciliopathies, e.g., polycystic kidney disease (PKD), polydactyly, diabetes, blindness, obesity, *situs inversus*, infertility, respiratory diseases, hydrocephalus, cognitive impairment, and developmental disorders [4, 7, 30, 31].

It has been suggested that there is a direct connection between primary cilium changes of length and bending in a local extracellular flow gradient and the sensory function of cilia [13, 30].
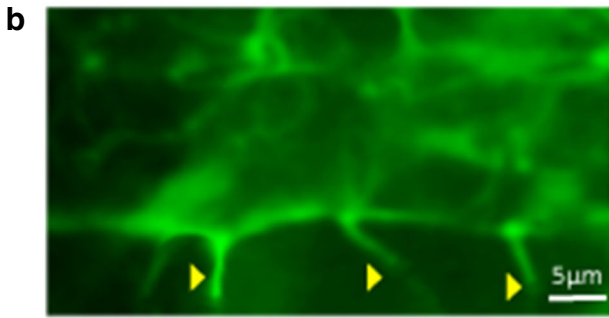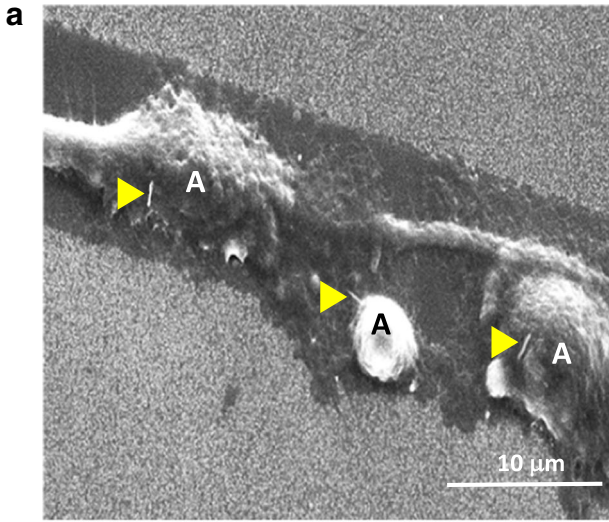
By courtesy of Prof Dr Acc. Maxwell Bennett
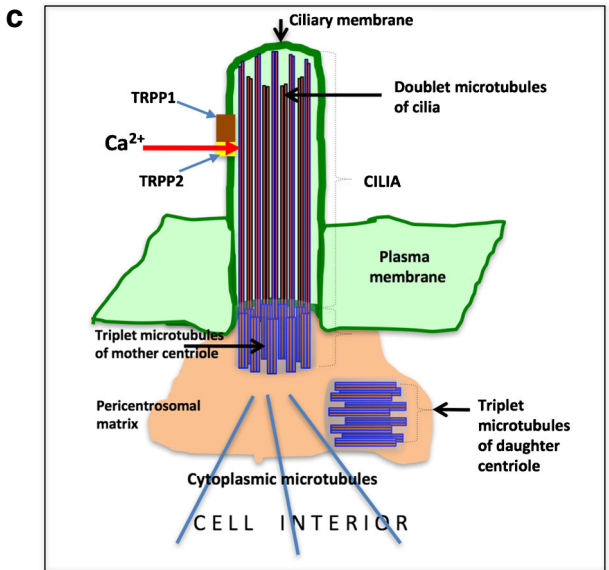
Fig. 1 Primary cilia (PC). **a** Primary cilia (▶) of astrocytes experimentally aligned in a lane by means of microchannels and visualized by scanning electron microscopy (SEM). **b** Primary cilia (▶) from the same preparation as depicted in **a**, but fluorescently labeled with BODIPY-cholesterol. **c** Primary cilia are connected via microtubule pathway systems to the cell interior. As a matter of principle, an environmental calcium-based signal, captured by calcium-based polycystin channels (TRPP1 and TRPP2), could be transmitted by this pathway wherever it is needed within the cell interior

1.2 Calcium entry into the primary cilium space triggers changes in primary cilium morphology and the microtubules-based skeleton

Recently, primary cilia have been recognized as 'specialized calcium-signaling organelles' [3]. Indeed, calcium-based channels (TRPP1/2) located within the primary cilia membrane and axonemal microtubules that possess numerous calcium binding sites constitute a necessary part of the primary cilia calcium signaling mechanism that processes calcium signals from the cellular environment into the intracellular space.

A large amount of a current research data indicates that the primary cilium responds to calcium entry by morphological adjustments [3, 32–39]. However, the precise molecular mechanism underpinning these changes remains to be elucidated. Although primary cilia are recognized as microtubule-based organelles and 'specialized calcium signaling organelles' [3], there are little data available to shed light on how calcium interaction with axonemal microtubules may have an important role in ciliary sensing. For example, a tight functional connection between calcium-based channels (polycystin 2 (TRPP2)) and calcium-binding axonemal microtubules has been revealed by the finding that the activity of the channel was rapidly decreased by the addition of the microtubule depolymerizing agent colchicine, while it was increased by the addition of the microtubule stabilizing agent paclitaxel [40].

The hypothesis to be tested by this study is that calcium may be the common causal denominator responsible for morphological changes of primary cilia and axonemal microtubules. Calcium that enters in the intra-ciliary space via mechanosensitive TRPP2 channels is likely to bind to axonemal microtubules within the cilia, increasing their flexibility, and resulting in a larger extent of bending and a shortening of the cilia.

2 Materials and methods

2.1 Cell culture

Mixed cultures of spinal cord glia were obtained from 12-h-old neonatal Sprague-Dawley rat pups by use of culture methods adapted from Scemes and colleagues [41]. To obtain a culture of astrocytes, further purification was performed using methods established elsewhere [42, 43].

To form a pattern of parallel astrocyte lanes on transparent microscopic coverslips, we employed a photolithographic micropatterning technique described elsewhere [44–48]. Briefly, a coverslip of 80-μm thickness was pre-covered with 20 μg/ml poly(D)lysine (Sigma). The mold of lithographically home-designed microchannels was premade in silicone elastomer Sylgard (Dow Corning, Midland, MI, USA). Using the patterned mold of microchannels, the appropriate pattern was transferred onto the coverslip. Thus, microchannels were formed whose poly(D)lysine base was ~20 μm wide and the microchannels were tens of microns long. The base of the lane was confined by the walls of 1.0% high-gelling temperature agarose
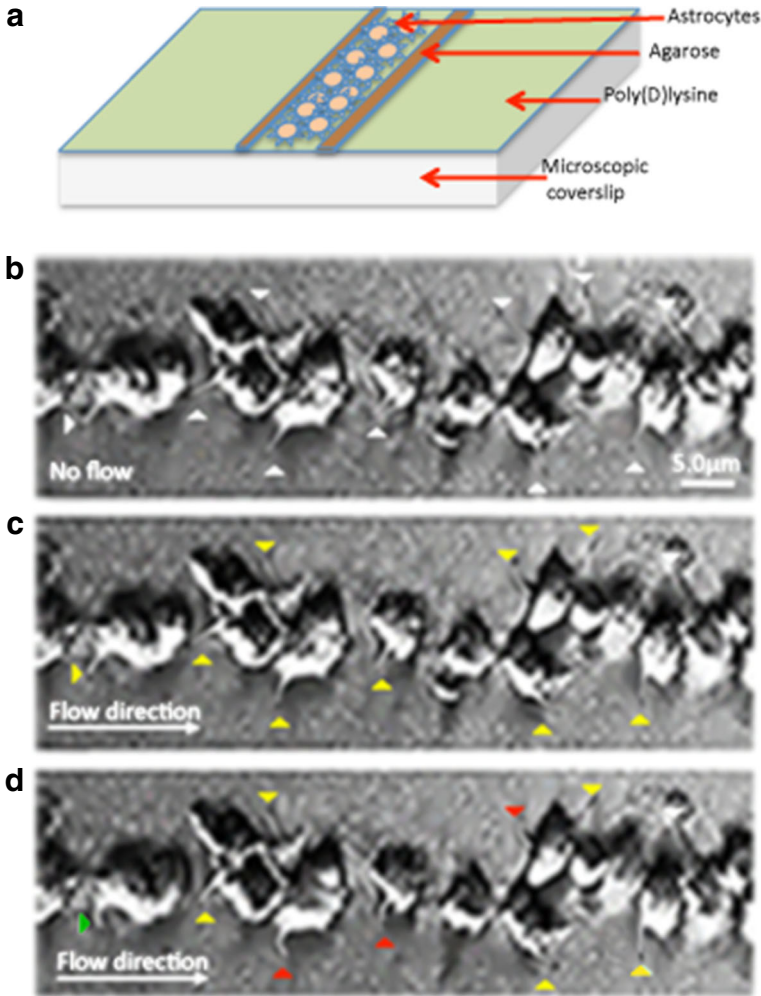
By courtesy of Prof Dr Acc. Maxwell Bennett

Fig. 2 Bending and shortening of astrocyte primary cilia. Thirty primary cilia were investigated in this experiment, with the images shown representing typical morphological changes of PC during the experimental procedures. **a** An illustration of the micropatterning technique employed in this work: astrocytes self-align in lanes within microchannels created by photolithography allowing primary cilia integrity to be preserved. **b** The 'lane cell culture' of astrocytes was equilibrated and oxygenated at 36°C in standard culture medium, unperturbed by any flow for 30 min. The *white arrowheads* indicate straight primary cilia – this was taken as the referential state of 100% straight primary cilia. **c** Aligned astrocytes were exposed to calcium-free flow (10 μl.s^{-1}) of cell culture medium for 15 min. The majority of primary cilia underwent two types of slight bending (*yellow arrowheads*). 15 min after flow stoppage, bent primary cilia returned to their straight shape. One mode of primary cilium bending is "slight" bending, which refers to the bending that happens gradually from its base up to its tip, while the other mode of bending is bending close to the base of the primary cilium, while the rest of its body is straight. d Aligned astrocytes were washed by flow (5 μl.s^{-1}) using standard culture medium for about 15 min. Astrocytes were subsequently exposed to medium flow (10 μl.s^{-1}) that contained 1.0 mM calcium for 15 min. The majority of primary cilia again became bent. However, some of them became "slightly" curved, similar to their appearance in the calcium-free flow (*yellow arrowheads*), while others were "strongly" curved (*red* and *green arrowheads*). There was also a subpopulation of shortened primary cilia among those that were strongly curved (*red*); 30 min after the flow had been stopped, the subpopulation of "strongly" bent primary cilia did not return to their straight shape, while the "slightly" bent subpopulation did (not shown)

(Sigma). Therefore, cells (astrocytes) can grow in the lanes formed by the poly(D)lysine path but are confined by the agarose walls (Fig. 2a).

The unlabeled primary cilia were observed as tiny cylindrical, slender protrusions of the membrane of the aligned astrocytes by using a scanning electron microscope (Philips XL 30 CP; University of Sydney, Australian Centre for Microscopy & Microanalysis) (Fig. 1a). Also, primary cilia were identified at the membrane of aligned astrocytes when cells were stained with BODIPY-cholesterol using an Ott-Lippincott-Schwartz protocol [49] and visualized by using a physiological fluorescence microscope (Olympus BX5OWI) (Fig. 1b).

To investigate and quantify the morphological changes of primary cilia of aligned astro-cytes under different conditions, we used the light mode of the fluorescence microscope. The biological viability of the cells arranged in lanes was successfully tested by calcium propaga-tion experiments as described elsewhere [45].

2.2 Exposing cultured cells to a flow of its medium

To generate the flow of cell culture medium in the cell culture chamber, we used an open perfusion system as described elsewhere [6, 35]. Flow rate was calibrated by the measurement of the efflux into a reservoir of known volume. Unless stated otherwise, we used a flow of rate of 10 $\mu l.s^{-1}$.

2.3 Reassembly of microtubules and ultrastructural examination

To reconstitute microtubules in vitro we used microtubule protein (MTP). MTP denotes a mix of tubulin and microtubule-associated proteins (MAPs). MTP was obtained from bovine brain by the temperature-dependent cyclic assembly/disassembly method, as described elsewhere [50]. MTP concentration was determined by the modified Lowry protein assay method, as described in the Pierce Instruction Manual (#23240; Pierce Inc., IL, USA). Using quantitative densitometric analysis of SDS-polyacrylamide gels, stained with Coomassie brilliant blue R-250, the MTP was shown to contain 95% tubulin and 5% MAPs, where percentages are calculated in terms of total MTP protein [50].

During cyclic preparation of tubulin, MAP-2 is by far the predominant MAP purified, since it is heat stable. Additionally, following purification, there was sufficient MAP-2 to bind along the entire microtubule length [51]. Moreover, the periodicity of the MAPs distribution and the length of the projections (~32 nm) in Fig. 8a and b correspond well to the MAP-2 superlattice [51].

We performed two sets of experiments: the first was related to microtubules of predomi-nantly straight morphology, while the second was related to microtubules of predominantly curved morphology. Unless stated otherwise, all experiments were performed under standard solution conditions, with microtubules reconstituted from MTP in MES buffer, containing (in mM): 100 MES, 1 EGTA, 0.5 $MgCl_2$, 1 GTP, pH 6.6. In the case of the first group, the buffer did not contain an excess of calcium. The second group of experiments was carried out in the presence of an excess of 1 mM $CaCl_2$, or as indicated in the text. The excess of calcium was added to the solution prior to microtubule assembly [52].

Microtubules were prepared for electron microscopy (EM) according to Langford's method [53]. Briefly, microtubules were reconstituted at the desired MTP concentration by leaving them to assemble for 60 min at 36 °C. Microtubules were fixed and stained with 2% uranyl acetate on '200 mesh grids'. Samples were left overnight at room temperature prior to

microscopic examination. Microtubule morphology was assessed using an analytical Philips CM12 transmission electron microscope (TEM) at the Australian Key Centre for Microscopy and Microanalysis, University of Sydney. EM Images were obtained using a Gatan multiscan CCD camera and an exposure time of 1.51 s.

2.4 Determination of lengths and extent of bending of microtubules and cilia

To determine the curvature of microtubules and primary cilia, a chosen curvature was approximated by a circle. The radius of the circle was measured by ImageJ-1.46r using the straight mode. Curvature was calculated as the inverse of the circle radii. The effective lengths were measured by ImageJ-1.46r using polygonal mode.

3 Results

3.1 Identification of primary cilia in the lane system of aligned astrocytes and comparison of the data obtained by other authors using different techniques

The presence of unstained primary cilia at the surface of aligned astrocytes was confirmed using scanning EM (Fig. 1a). BODIPY–cholesterol staining permitted identification of primary cilia, including morphological detail of the head-end of the tip of the primary cilia (Fig. 1b). On the other hand, primary cilia, when not stained, were still easily visualized due to their distinctive head-end-morphological features, in particular when extending laterally out of the lane. Therefore, we continued our observations of primary cilia by the microchannel technique without staining them (Fig. 2b, c, and d and Fig. 3a, b, and c).

The preliminary data obtained from astrocytes aligned by microchannels, using electron scanning and fluorescence microscopic techniques, show that primary cilia length is on the scale of several micrometers, while average diameter is approximately 250 nm (Fig. 1a, b). These data are in good agreement with the results obtained in other different systems by other authors [1–3].

3.2 Morphological changes in primary cilia under different experimental conditions defined by medium flow, calcium, and taxol

To observe morphological changes in primary cilia which were instigated by calcium, we utilized the lanes of astrocytes prepared according to the procedure illustrated in Fig. 2a.

3.2.1 Bending

We performed the same experiment on 30 astrocytic primary cilia in total, but divided the experiments into four batches. One batch of aligned astrocytes was removed from the incubator and was immediately placed in the experimental chamber on the microscope stage and left to equilibrate with oxygenation at 36 °C for 30 min (Fig. 2b). After 30 min of equilibration, primary cilia of straight morphology were monitored and an image was taken for length measurement. The system was then exposed to a flow ($10 \ \mu l.s^{-1}$) of calcium-free culture medium (containing 1 mM EGTA) for 15 min. Although a majority of morphologically straight primary cilia were changed into a curved morphology within the first 30 s, we
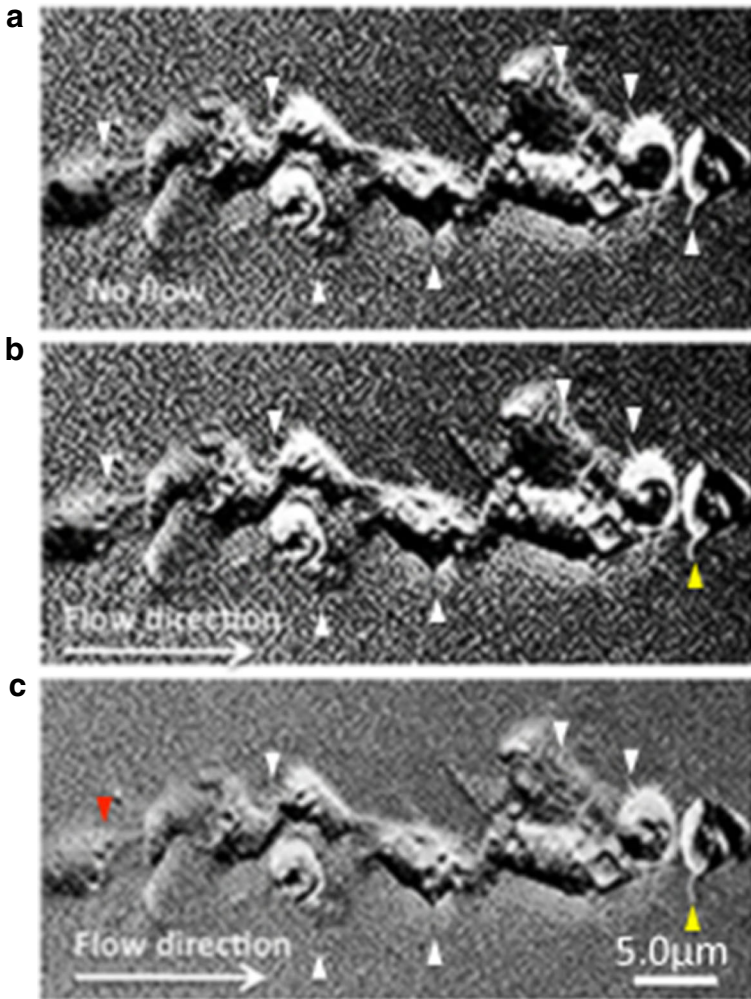
By courtesy of Prof Dr Acc. Maxwell Bennett

Fig. 3 Taxol attenuates primary cilium curving caused by calcium and flow. **a** Astrocyte cultured and allowed to stabilize in medium for 15 min, as in Fig. 3b. No flow, no taxol, or no calcium was applied. **b** 15 μM taxol was applied for 60 min in the absence of flow, followed by flow for 10 min, as in Fig. 3c. A small number of primary cilia underwent the "slight" mode of curving (*yellow arrowhead*) but significantly less than in the absence of taxol. **c** 1 mM CaCl$_2$ was subsequently infused for 30 min in the absence of flow. Calcium was then continuously infused with flow for 10 min, as in Fig. 3d. A small number of primary cilia underwent both "slight" and "strong" modes of curving (*yellow* and *red arrowheads*), but significantly less than in the absence of taxol

measured curvatures 15 min after flow initiation when 90% of primary cilia were bent. An exemplar can be seen in Fig. 2c. The average curvature of primary cilia was $2.1 \pm 0.89 \times 10^{-4}$ nm^{-1} and the curvature frequency distribution is shown in Fig. 4a(a); *black triangles*). The percentages of reversible slight bended population of primary cilia are shown in Fig. 5b (b1, b2). Fifteen minutes after the flow was stopped, all bent primary cilia had reassumed their straight form (results not shown).

To eliminate EGTA, the system was washed in flowing (5 μl.s^{-1}) standard cell culture medium for 10 min. The system was then left without any flow for 15 min, ensuring that all
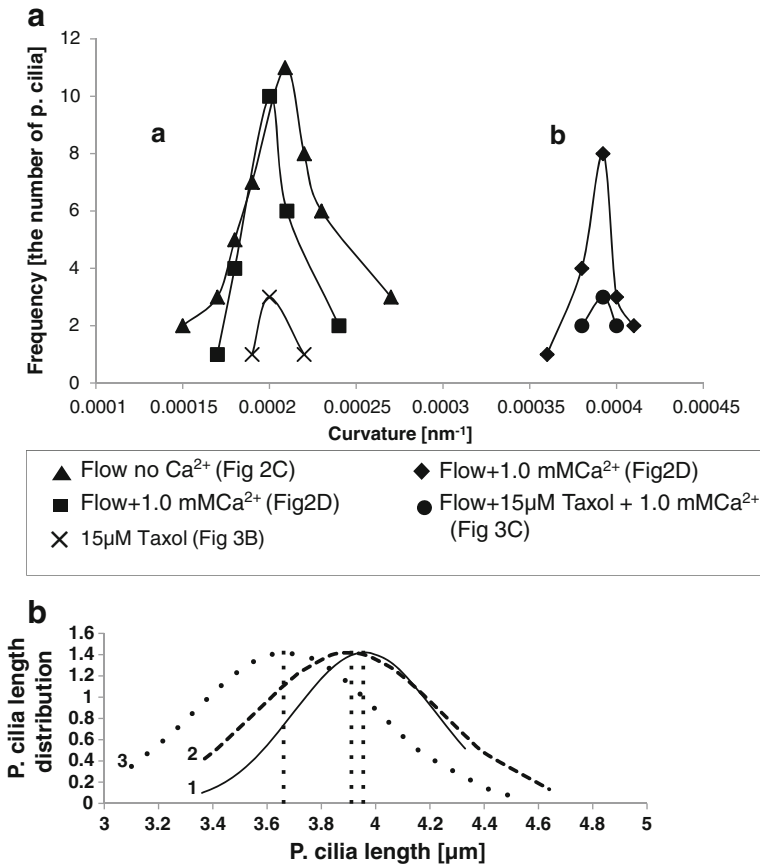
Fig. 4 Quantitation of the effects of flow, calcium, and taxol on the curvature and length of primary cilia (from Figs. 2 and 3). **a** The frequency of curvature distribution shows two distinct curvature groups, 'slight' curvature and 'strong' curvature. (a) The 'slight' curvature occurs at <0.0003 nm^{-1}, with an average curvature distribution centered at ~0.0002 nm^{-1} and was observed during flow (10 $\mu l.s^{-1}$) in the absence of calcium ($\blacktriangle$; Fig. 2c), in 1 mM calcium ($\blacksquare$; Fig. 2d), or in the presence of 15 μM taxol ($\mathbf{X}$; Fig. 3b). (b) The 'strong' curvature occurs at >0.0003 nm^{-1}, with an average curvature distribution centered at 0.00039 nm^{-1} and was observed during flow (10 $\mu l.s^{-1}$) in the presence of 1 mM calcium ($\blacklozenge$; Fig. 2d), or in the presence of 15 μM taxol and 1 mM calcium ($\bullet$; Fig. 3c). **b** The length distribution of primary cilia decreased in the presence of both flow and calcium: 1. Average cilia length was 3.96 ± 0.2 μm (1 ——) in the absence of flow and calcium (Fig. 2b). 2. Average cilia length was 3.90 ± 0.2 μm (2 - - - -) in the presence of flow (10 $\mu l.s^{-1}$) but the absence of calcium (Fig. 2c). 3. Average cilia length was 3.67 ± 0.2 μm (3 ·······) in the presence of flow (10 $\mu l.s^{-1}$) and 1 mM calcium (Fig. 2d)

primary cilia reassumed a straight morphology. Medium containing 1 mM CaCl$_2$ was then flowed with a rate of 10 $\mu l.s^{-1}$. After 15 min, primary cilia morphology was observed and an exemplar is shown in (Fig. 2d). The majority (90%) of the primary cilia had undergone bending within the first 30 s. However, at the end of 15 min, 50% of them were slightly curved, which was similar to that seen in the calcium-free flow (Fig. 2d; yellow arrowheads). The associated frequency curvature distribution is show at Fig. 4a(a); black squares). The rest of the primary cilia (40%) were bent to a greater extent (Fig. 2d; arrowheads). The average curvature of these strongly bent primary cilia was $3.9 \pm 0.115 \times 10^{-4}$ nm^{-1} and the associated curvature distribution is shown in Fig. 4b(b); black diamonds). The percentages of the bent population of primary cilia are shown in Fig. 5c (c1, c2).
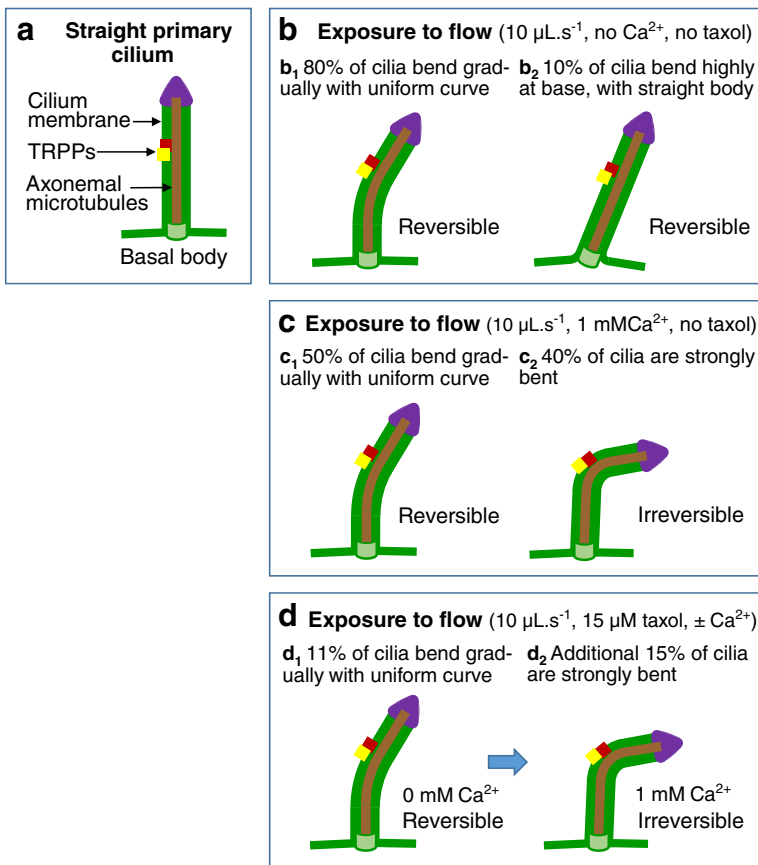
Fig. 5 The population of different curving modes. These diagrams summarize the key outcomes of the experiments shown in Figs. 2, 3 and 4. **a** The primary cilium is straight under conditions of no flow, no taxol, and no calcium. **b** When flow of medium is applied (10 μl.s^{-1}), 80% of cilia bend 'slightly', exhibiting a gradual, uniform curvature from the bottom to their top (b$_1$), while 10% of cilia bend by tilting at their base, while the body of the cilium remains straight (b$_2$). 10% of cilia did not bend (see also Fig. 3b). **c** When 1 mM calcium was present in the flow (10 μl.s^{-1}), 40% of cilia 'slightly' bent, gradually from the bottom to their top (c$_1$) and 50% of cilia bent 'strongly', approximately half way along their length, while the shape of 10% of cilia remained unchanged (see Fig. 3c). **d** After incubation with 15 μM taxol for 60 min, 11% of cilia curved 'slightly' and reversibly by during flow of medium (10 μl.s^{-1}) (d$_1$). Following subsequent incubation with 1 mM calcium for 30 min, an additional 15% of cilia appeared 'strongly' and irreversibly curved within the flow of medium (d$_2$)

We monitored the cells for 30 min after the flow had stopped and noted that the subpopulation of the more strongly bent primary cilia had not reassumed their straight form, while those less bent did (not shown). Here the term 'strong' bending denotes that the associated curvature is greater than 2×10^{-4} nm^{-1}, or else the bending is referred to as 'slight' bending.

3.2.2 Taxol effect

To investigate the effects of the microtubule stabilizer, taxol, on morphological changes of primary cilia of astrocytes aligned in the lane, we prepared the astrocyte cell culture as shown in Fig. 2a, and allowed it to stabilize in the medium as in Fig. 2b, for 15 min: no flow, no taxol, no calcium was applied (Fig. 3a). In the next step, 15 μM taxol was applied for 60 min in the

absence of flow. No morphological changes were observed (not shown). Subsequently, flow was applied (maintaining the same concentration of taxol) for 10 min (Fig. 3b). A small number of primary cilia underwent slight curving (Fig. 3b; yellow arrowhead), but significantly less than in the absence of taxol. The curvature frequency distribution is shown in Fig. 4a(a); (x) and Fig. 5d(d_1). The effect of calcium was then observed by infusing 1 mM calcium for 30 min by flow (Fig. 3c). A small number of primary cilia underwent slight curving (yellow arrowhead) and a strong mode of curving (red arrowhead), but significantly less than in the absence of taxol. Quantitative data are shown in Fig. 4a(b); black circles) and Fig. 5d(d_2).

3.2.3 Length of primary cilia

Apart from the primary cilia curvature, it was also apparent that the length distribution varied under the different experimental conditions. Measurements showed that the length of primary cilia was shifted toward shorter values in the presence of excess calcium during flow (Fig. 4b). The average length of primary cilia was found to be 3.96 ± 0.26 μm in the absence of flow and without an excess of calcium (Fig. 4b(1)). The average length of primary cilia was 3.90 ± 0.34 μm in calcium-free flow experiments (10 μl.s^{-1}) (Fig. 4b(2)) and 3.67 ± 0.34 μm during flow (10 μl.s^{-1}) in the presence of 1.0 mM calcium (Fig. 4b(3)). Shortening of primary cilia was detected among 20% of the stronger curved primary cilia (Fig. 2d; red arrowhead); Fig. 4b(3)).

3.2.4 The degree of primary cilia bending varies in different solution conditions: An illustration

The experiments with calcium indicated that the biophysical character of morphological changes of primary cilia in the presence of excess calcium is different from those in the absence of calcium, caused by medium flow alone. Furthermore, taxol attenuates primary cilia morphological changes caused by flow and calcium. We have summarized these changes in an empirical model (Fig. 5). This demonstrates that primary cilia are capable to sense fine changes in solution conditions, as indicated by the appropriate degree of bending. Moreover, taxol experiments indicate that this primary cilia function is directly related to appropriate morphological changes of axonemal microtubules.

3.3 The molecular mechanism of primary cilia bending following calcium binding to axonemal microtubules

We have hypothesized that excess calcium can induce primary cilia bending and shortening by calcium binding to axonemal microtubules causing bending and shortening of these microtubular structures.

It has been previously shown that an excess of calcium cations can induce microtubule shortening in the absence of MAPs or bending in the presence of MAPs in vitro [52, 54]. Therefore, it is reasonable to assume that bending or shortening of primary cilia may be primarily driven by bending or shortening of its axonemal microtubule skeleton after calcium entrance into the ciliary space via calcium-based channels TRPP1/2 and calcium binding to axonemal microtubules (Fig. 1c; Fig. 5).

The following experiments were undertaken to investigate this hypothesis: (1) effect of taxol on primary cilia morphology versus calcium effect, (2) a re-investigation of the

effect of excess calcium on curved microtubule morphology under in vitro conditions, (3) an investigation to determine whether the size of the resulting microtubule curvatures are correlated with the primary cilia curvatures and (4) an estimation of the required calcium entrance via calcium-based TRPP1/2 channels to produce the obtained curvatures.

3.3.1 Taxol attenuation of primary cilia morphological changes caused by flow and calcium

Taxol is known as microtubule structure stabilizer [55–58]. As described in the previous section, we have shown that taxol attenuates calcium- and flow-mediated morphological changes of primary cilia (Fig. 3c; Fig. 4a (x), 4b, black circles); Fig. 5(d)).

3.3.2 Excess calcium induces microtubule bending in vitro

Microtubules were reconstituted in vitro, under controlled conditions, which excluded excess calcium ($[CaCl_2] = 0$ mM, $T = 36$ °C as described in Materials and methods). At a microtubule protein (MTP) concentration of 7.0 mg/ml, the majority of straight microtubules spontaneously undergo self-organization, which results in bundle formation (visualized by TEM; Fig. 6a(a)). Furthermore, Fig. 6(b) is the same specimen as in Fig. 6(a), but seen at higher exposure. Here one can see highly aligned straight microtubules within the bundle, which are spatially separated from non-aligned curved microtubules. Since there was no artificial local flow in the sample, the most likely explanation is that this very local separation of straight from curved microtubules was produced by a spontaneous phase separation mechanism, as has been observed previously under similar solution conditions [52].

To observe the effect of calcium on microtubule morphology and self-organization, microtubules were prepared under the same conditions as in Fig. 6a(a), except for the addition of excess calcium. Fig. 6b(a, b) shows microtubules prepared in the presence of a variable concentration of calcium as follow: Fig. 6b(a) (0.5 mM $CaCl_2$, 3 mg/ml MTP), while Fig. 6b(b); (1.5 mM $CaCl_2$, 3 mg/ml MTP).

Fig. 6b(a) (0.5 mM $CaCl_2$) shows a mixed population of straight and curved microtubules, where straight microtubules are undergoing a phase separation, characterized by straight microtubules forming a pattern of parallel microtubules within their domains, while curved microtubules have formed a pattern of entangled microtubules within their domains. At higher calcium concentration (1.5 mM), only multiple curved microtubules appear (shown at Fig. 6b(b)). Bars correspond to either 0.3 μm (Fig. 6a(a,b)) or 5.0 μm (Fig. 6b(a,b)).

3.3.3 Basic architectural-structural considerations of microtubule curving

Under the experimental conditions described above for Fig. 6b(b) (Material and methods; 2 mg/ml MTP; 1.5 mM $CaCl_2$), and using TEM, we have found that microtubules undergo curving in vitro, due to calcium action. The population of curved microtubules bifurcates into two microtubule sub-populations with distinctly different curvatures (Fig. 7a, b, and c). The first sub-population has an average curvature of $5.71 \pm 0.16 \times 10^{-3}$ nm^{-1} with an associated average radius of 145 nm (Fig. 7b(a)). The
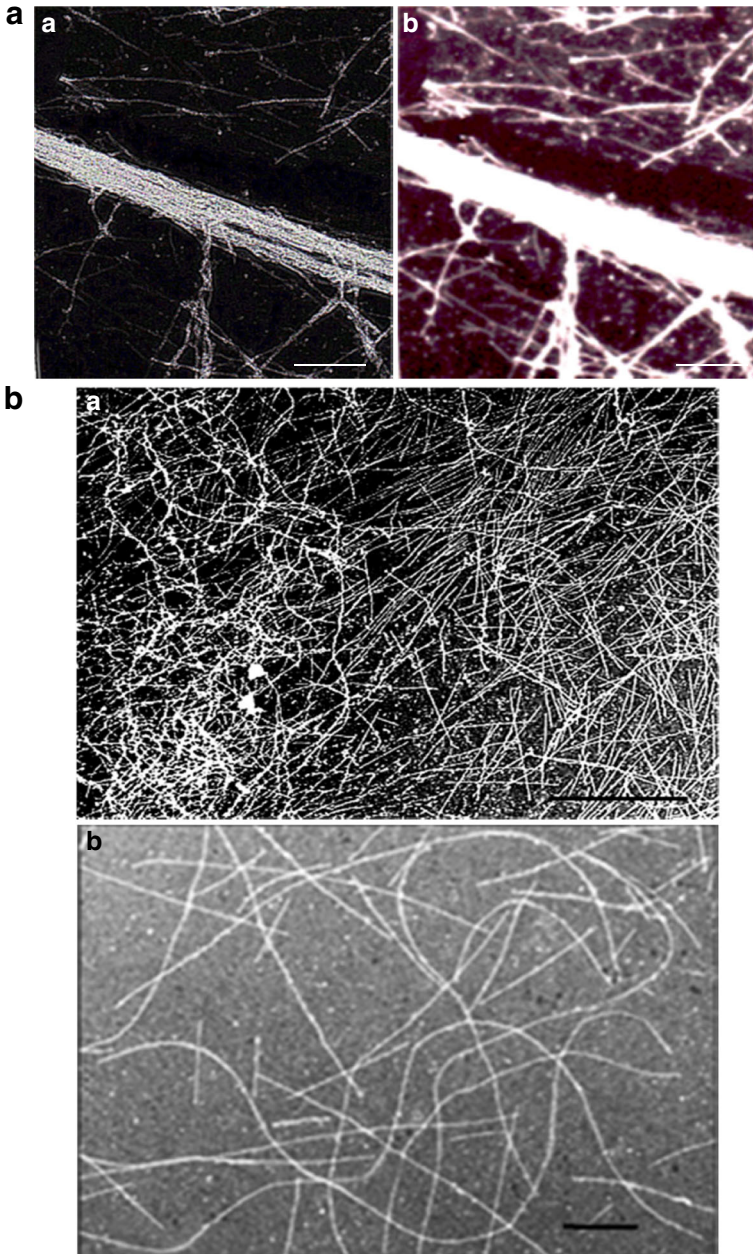
Fig. 6 Transmission electron microscopy reveals phase separation of self-aligned straight microtubules from self-entangled curved microtubules – the effect of calcium. **a** Microtubules were prepared in vitro, in the absence of calcium, at 36 °C (a). Mainly straight microtubules spontaneously self-organized in bundles. Microtubule protein [MTP] concentration 7.0 mg/ml. (b) The same sample as in (a) but at higher exposure in order to visualize the spontaneous phase separation of bundled self-ordered phase of straight microtubules from the disordered phase of curved microtubules. *Bars* correspond to 0.3 μm. **b** The addition of calcium to the MTP alters both microtubule morphology and self-organization. (a) Following the addition of 0.5 mM CaCl$_2$, the populations of straight and curved microtubules underwent a phase separation. Straight microtubules align and form separate domains from the one-fold-curved microtubules, which become entangled in their own domains. [MTP] = 3 mg/ml. (b) Following the addition of 1.5 mM CaCl$_2$, microtubules appeared multiply curved with no phase separation seen. [MTP] = 2.0 mg/ml. *Bars* correspond to 5.0 μm

second sub-population had a larger curvature of $(10 \pm 0.5 \times 10^{-3}$ nm^{-1}, with an associated average radius of 100 nm (Fig. 7b(b)). The frequencies of both curvature distributions are shown in Fig. 7c.

Our data also show some defects in the super-lattice structure of MAPs including detachment of MAPs, accompanied by regional microtubule bending caused by calcium binding to either MAPs or $\alpha\beta$-tubulin dimer, or to both (Fig. 8a, b).

3.3.4 Pappus centroid theorem - application

On the basis of the data in Fig. 7a, b, and c and Fig. 8a and b, the basic architectural-structural arrangements can be schematically illustrated as shown in Fig. 9a, b, and c. An estimation of the average number of tubulin dimers that occupy the curved part of a microtubule, as well as the number of MAPs that stabilize microtubule curvature, is made on the basis of an approximation of the curved part of the microtubule with toroid section (Fig. 9c). Using Pappus' centroid theorem [59] the surface of the toroid section (S) is calculated by the formula

Fig. 7 The one-fold-curved microtubules. **a** 2 mg/ml MTP in 1.5 mM CaCl$_2$ was viewed by TEM. Two subpopulations of one-fold-curved microtubules show distinctly different curvatures. *Bar* is 0.3 μm. **b** The detail (taken from (a) is an example of the measurement of radii of two typical microtubule curvatures. The *circles* were inserted to best correspondence with the relevant arc-length of the curvatures. The smaller curvature (a) is 0.0057 ± 0.0002 nm-1 with an associated average radius of 175 nm, and a central angle of 90.08°. The larger curvature (b) is 0.01 ± 0.0005 nm-1, with an associated average radius of 100 nm, and a central angle of 130°. *Bar* is 0.2 μm. **c** Frequency distributions of the smaller (●) and larger (■) curvatures
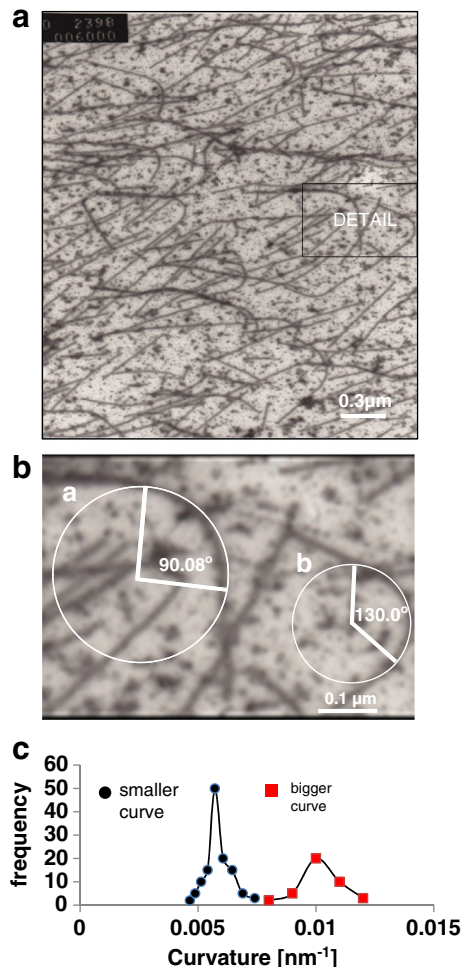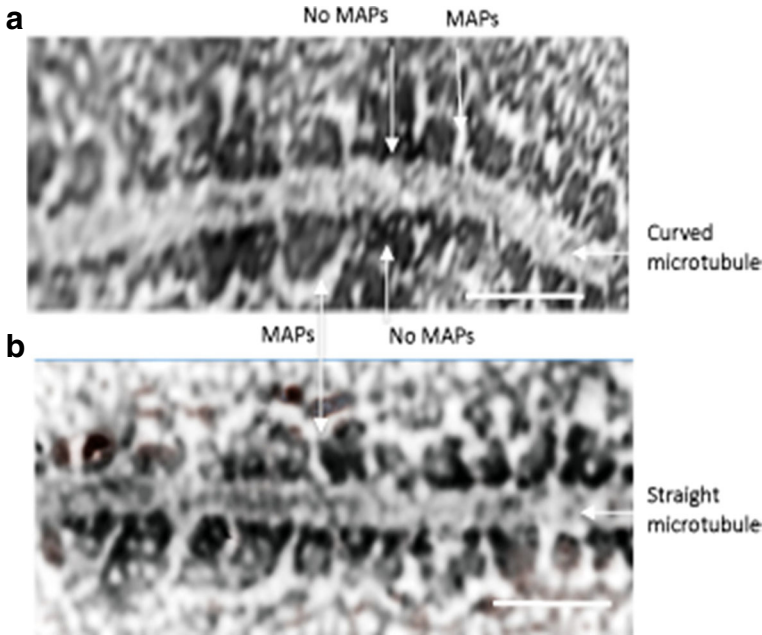
Fig. 8 Calcium may induce microtubule curving by partial or complete dislocation of MAPs. **a** Microtubule curvature is formed where MAPs are lost completely or partially [92, 93]. **b** For comparison, a straight microtubule appears to have all MAPs present. The periodicity of MAPs distribution and the length of projections (~32 nm) correspond to the MAP-2 superlattice [51, 94]. *Bar* is 50 nm

$$S = 2\pi \times \theta \times R \times r \tag{1}$$

Fig. 9 The basic architectural considerations of microtubule bending. The degree to which a microtubule can be bent is determined by a combination of intrinsic mobility of the GDP-$\alpha\beta$-tubulin dimer within the protofilament and the presence/absence of MAPs. **a** (a) The straight microtubule protofilament constituted by GTP-$\alpha\beta$-tubulin dimers and stabilized by MAPs. (b) The straight microtubule protofilament constituted by GDP-$\alpha\beta$-tubulin dimers exhibit two degrees of freedom of motion within the protofilament: rotation about the axis between neighboring dimers ≤24°, and it may rotate between its subunits ≤27° [77]. These motions may allow the protofilament to bend, although MAPs will stabilize the protofilament against bending. (c) Calcium binding to MAPs loosens MAPs interaction with GDP-$\alpha\beta$-tubulin dimers, allowing the protofilament to undergo curving ≤24° between related neighboring GDP- $\alpha\beta$-tubulin dimers. (d) Calcium binding to both MAPs and to GDP-$\alpha\beta$-tubulin dimers loosens MAPs interaction and also allows tubulin subunits (α and β) to undergo a rotation with respect to each other ≤27°. **b** The behavior of the basic microtubule architecture during bending is illustrated by considering the motion of the two opposite protofilaments (X,Y) within the microtubule wall, allowing a freedom of rotation of neighboring dimers relative to each other of 24°. (a) Two protofilaments (X, Y) within the microtubule wall are positioned opposite to each other at a distance of 15 nm. (b) To conserve the diameter of the microtubule, when protofilament Y is curved by the rotation of one GDP-$\alpha\beta$-tubulin dimer (*blue*) by 24°, the curving is automatically accompanied by the curving of protofilament X by rotation of two tubulin dimers (*blue*). (c) If microtubule curvature involves an angle greater than 24° then protofilament Y utilizes two successive rotations (each one is 24°) of two tubulin dimers (*blue*). In order to maintain the internal diameter of the microtubule, this is accompanied by the rotation of four tubulin dimers of protofilament X. Hence, the concave curvature of protofilament Y and the corresponding convex curvature of protofilament X may be expressed in terms of accompanied radii as: $R_Y \approx 2.5$ tubulin dimers ≈ 19.5 nm, associated concave curvature is ≈ 0.051 nm^{-1}; while for the convex curvature $R_X \approx 4.0$ tubulin dimers ≈ 31.2 nm and associated convex curvature is ≈ 0.032 nm^{-1}. **c** Finally, a curved part of the microtubule can be approximated by the toroidal section to calculate the surface area by applying Pappus' centroid theorem (see Eq. 1) [59]
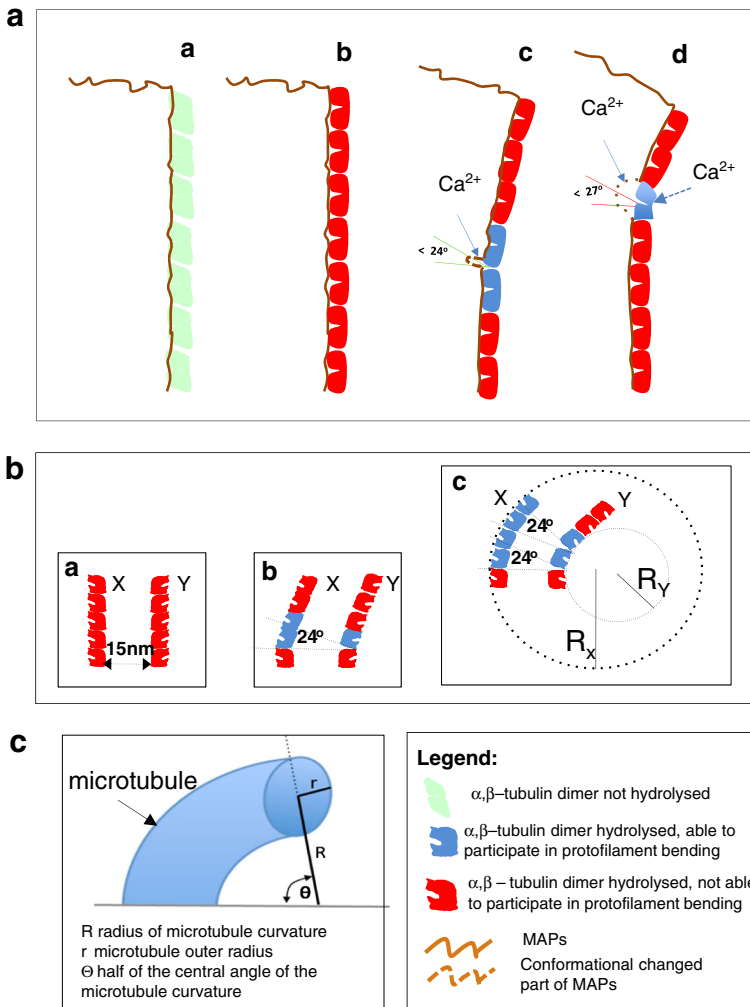
Here θ is half of the central angle (measured in radians) associated with the curvature, R is the average radius (measured in nanometers) of the curvature, and r is the external radius of the microtubule (12.5 nm) (Fig. 9c).

Regarding the smaller curvature, the measured half central angle $\theta = 0.786$ rad (45.04°) and the radius of the curvature $R = 145 \pm 12.5$ nm (from Fig. 7b(a)). According to formula (1), the size of the surface of the curved (toroid) section S is 8943 nm^2. If a tubulin dimer is approximated by a cylinder, then the dimensions of the surface of its central axial intersection are 4 nm × 7.8 nm. Consequently, the size of the surface of the intersection is 31.2 nm^2. Here we did not take into account the gap between neighboring (in the axial direction) tubulin dimers. Therefore, the number of tubulin dimers that can be accommodated by this toroid section is 8943 nm^2 / 31.2 nm^2, i.e., 287 tubulin dimers. On the other hand, this toroid section is constituted by 13 curved microtubule protofilaments. Therefore, on average 22 tubulin dimers are accommodated by each protofilament of a curved (toroid) region for microtubules exhibiting a smaller curvature.

Regarding the bigger curvature, the measured half central angle $\theta = 1.134$ rad (65°) and the radius of the curvature is $R = 100 \pm 12.5$ nm (from Fig. 7b(b)). The surface of the curved (toroid) section S is 8901 nm^2. The number of tubulin dimers that can be accommodated by this toroid section is 8901 nm^2 / 31.2 nm^2, i.e., 285 tubulin dimers. Consequently, 22 tubulin dimers are accommodated by each protofilament of a curved (toroid) region for microtubules exhibiting a bigger curvature.

3.3.5 Contribution of calcium interaction with αβ-tubulin dimer in generating the microtubule curvatures

Based on the number of αβ-tubulin dimers calculated above to be involved in the formation of the bigger/smaller curvatures, the number of calcium cations that can participate, via binding to αβ-tubulin dimers, in the formation of these curves can be calculated. There are 18 calcium binding sites on each αβ-tubulin dimer [60–62]. If all tubulin calcium binding sites have to be occupied to create the bigger curvature, then 285×18, i.e., 5130 calcium cations are required. Concerning the smaller curvature, the same rationale, i.e., 287×18 gives 5166 calcium cations that participate in the formation of a smaller curvature via calcium binding to αβ-tubulin dimers.

3.3.6 Contribution of calcium interaction with MAPs in generating the microtubule curvatures

This architectural-structural data allows an estimation of the contribution of MAPs to microtubule curvature stability. Linker MAPs, or microtubule stabilizers, have an average length of 100 nm and are located mainly along the microtubule grooves [63]. An estimate of the number of linker MAPs involved in stabilizing the bigger/smaller microtubule curvatures are as follows: 22 tubulin dimers span approximately 171 nm, consequently 1.71 linker MAPs may be accommodated per one groove, or 22 linker MAPs in total per curved part of the bigger microtubule curvature, in order to stabilize it. Concerning the smaller curvature, 22 tubulin dimers span along 172 nm, hence, in order to stabilize the smaller curvature, 1.72 linker MAPs may be accommodated per single groove or 22 linker MAPs per curved (toroid) part of the smaller curvature.

Based on the number of linker MAPs calculated above to be involved in the formation of the bigger/smaller curvatures, the number of calcium cations that can participate, via binding to the linker MAPs, in the formation of these curves can be calculated. There are three calcium binding sites per one molecule of MAP-2 [64].

If all MAP-2 calcium binding sites have to be occupied to create the bigger curvature, then 22×3 i.e., 66 calcium cations are required. Concerning the smaller curvature, the same rationale i.e., 22×3 gives 66 calcium cations that participate in the formation of a smaller curvature via calcium binding to MAP-2, consequently loosening interaction with the corresponding αβ-tubulin dimers.

3.3.7 The maximal number of calcium cations engaged in primary cilium curving is negligible versus the capacity of TRPP1/2 calcium channels

Due to an abundance of calcium binding sites distributed over the αβ-tubulin dimers and associated MAPs, calcium effects within the microtubule system are versatile and

quite complex. The calcium that we propose acts upon the axonemal microtubules enters the internal space of the primary cilium by means of its TRPP1/2 channels. On the basis of our data, up to approximately 10,428 calcium cations are required to generate the average curvature of a single microtubule.

In making these calculations, we assume that the average curvature of a microtubule used in the calculations above is equivalent to that of a primary cilium, which contains nine doublet microtubules within the axonemal system of the primary cilium (approximately equivalent to 18 microtubules). Thus, we calculate that approximately 18 times more calcium will be required to generate primary cilium curvature compared to that for a single microtubule, which is equivalent to 1.88×10^5 calcium cations.

However, our results show that an average microtubule curvature, caused by calcium, is 7.9×10^{-3} nm^{-1} while the average curvature of a primary cilium caused by a similar excess of calcium is 3.9×10^{-4} nm^{-1} (Fig. 10). Thus, the average curvature of a primary cilium is about 20 times smaller than the average microtubule curvature. Therefore, following the reasoning used before, approximately 20 times more GDP-$\alpha\beta$-tubulin dimers constitute primary cilium curvature (the smaller curvature requires the involvement of a larger number of GDP-$\alpha\beta$-tubulin dimers – see Fig. 9b(c)). Therefore, we calculate that $20 \times 1.88 \times 10^5 = 3.75 \times 10^6$ calcium cations are engaged in generating primary cilium curvature in vivo.

The capacity of a TRPP1/2 channel is 5.42×10^{17} calcium ions that can be transported by TRPP1/2 [65]. This number overcomes 1.45×10^{11} times the maximal number of calcium cations necessary to create primary cilium curvature. This is in agreement with the finding that TRPP1/2 channels can supply sufficient calcium ions to cause primary cilium curving without significantly disturbing global levels of cytoplasmic calcium as recently suggested [66].
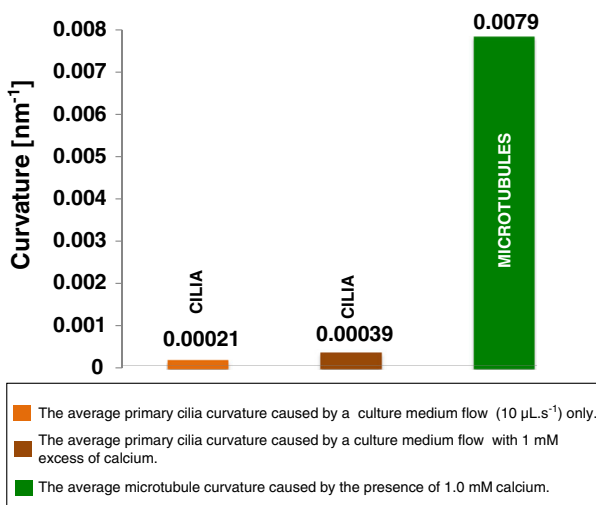

Fig. 10 Calcium instigates bending of both primary cilia and microtubules. The average curvature of a single microtubule is about 20 times stronger than the curvature of the primary cilia

4 Discussion

In this work, we address the question of biophysical mechanisms underlying primary cilia morphological changes, such as bending and length changes, in terms of axonemal microtubules bending and changes in length in response to calcium binding to their surface, i.e., to $\alpha\beta$-tubulin dimers and microtubule-associated proteins (MAPs).

4.1 Calcium instigated morphological changes of primary cilium

Our data show that calcium is able to mediate changes in the morphological and biophysical properties of primary cilia subjected to flow, by altering both the extent of bending and the length of the primary cilia. In calcium-free flow medium, the response by primary cilia was quite homogeneous, with 90% becoming "slightly" curved, i.e., there was only a small amplitude change in curvature. This "slight" bending was reversible and no change in the length of the primary cilia was observed. The remaining 10% of primary cilia did not respond to flow. However, in calcium-enriched flow medium, there was a bifurcation of response. 90% of the primary cilia became curved, but 50% demonstrated "slight" bending and 40% demonstrated "strong" bending. Additionally, the length of the primary cilia was reduced by 6% in the presence of calcium within the flow medium.

4.2 The bending of axonemal microtubules caused by binding of calcium cations underlies bending of primary cilia: Taxol effects

Although numerous research data have illustrated that calcium may be involved in primary cilium morphological changes (see Introduction), the molecular mechanism of this is still elusive. The only data (to our knowledge) that show a direct correlation between calcium entry in primary cilium intra-space and the behavior of axonemal microtubules was produced by Montalbetti and colleagues [40]. By examining calcium interaction with the primary cilium axonemal microtubule system, the role of calcium as a signaling molecule that may be able to control the dynamics of primary cilium morphological changes may be revealed, allowing further elucidation of its integration into subsequent cellular signaling events.

Axonemal microtubules constitute the primary cilium skeleton, occupying a large part (~70%) of primary cilium intra-space. Calcium may directly interact with the axonemal microtubules system after entering into the primary cilium intra-space via calcium-based TRPP1/2 channels. Changes in calcium concentration within the primary cilium intra-space can occur without substantially altering the global cytoplasmic calcium [2]. Within the primary cilium intra-space, calcium may interact with numerous negatively charged cationic sites (specialized for Ca^{2+} binding) located at the surface of the $\alpha\beta$-tubulin dimer [60–62, 67]. However, there are also three strong calcium binding sites MAP-2 [64, 68]. Additionally, previous data have shown that calcium may can cause microtubule shortening in the absence of MAPs and can induce bending in the presence of MAPs [52, 54].

Having demonstrated a direct effect of calcium on primary cilia morphology, we have replicated and quantitated these effects on isolated microtubules in vitro, to determine the quantity of calcium required within a cilium intra-space to mediate structural change in the axonemal microtubules, such as curving and shortening. By pharmacologically targeting axonemal microtubule structure with the microtubule stabilizer, taxol, we have substantially attenuated the morphological/structural effects that we propose are mediated by cilium intra-space calcium.

4.2.1 Interaction of calcium with microtubules in vitro in the presence of MAPs induces microtubule bending

We have shown that increased calcium concentration produces microtubule bending in the presence of MAPs in vitro. Bending appears to be single-fold when the calcium concentration is about 1 mM or less, but becomes multiple-fold at a higher calcium concentration (Fig. 6b). Furthermore, at intermediate calcium concentrations, a mix of straight and curved microtubule populations may exist. We propose that a phase separation mechanism may spatially separate these populations (Fig. 6a, b), in agreement with previous data [52], and consistent with the population of calcium-free microtubules being more rigidly straight. This finding supports a direct connection between calcium as a signaling molecule and spatial re-organization of cellular substructures such as microtubules. Indeed, this observation may be an example of calcium signaling integration, where calcium initiates events in the primary cilium that are subsequently transmitted deeper into the cell via a chain of intracellular microtubules.

Our data also demonstrate that within the curving region of the microtubule in vitro, MAP-2 is partially or completely dislocated (Fig. 8). We propose that calcium binding to MAP-2 leads to a weakening of the MAP-2-microtubule interaction. MAP-2 is a microtubule stabilizer, hence dissociation of MAP-2 from the microtubule following calcium binding supports the hypothesis that microtubule bending is, in part, mediated via disruption of MAP-2 interaction with the microtubule. However, this does not preclude microtubule curving due to the interaction of calcium directly with $\alpha\beta$-tubulin dimers.

Calcium effects on microtubule structure and dynamics encompass a range of other possibilities that also need to be considered. For example, the tubulin C-terminal tail is composed of a highly negative amino-acid sequence, and extends away from tubulin by ~4.5 nm. Calcium binding to the tail instigates its compaction that is essential for MAPs interaction with microtubules [69, 70]. Additionally, calcium may interfere with electric energy transfer by microtubules [71]. Calcium binding to $\alpha\beta$-tubulin dimers and MAPs may also play a critical role in the activation of nano-pores [72, 73]. Nano-pores are located between neighboring tubulin dimers, which belong to the neighboring microtubule protofilaments [74]. Nano-pores are believed to play a role as biological switches [72, 75, 76].

4.2.2 Taxol attenuates primary cilium curving caused by calcium

The microtubule stabilizer, taxol, promotes the assembly of microtubules in the presence of agents capable of causing disassembly, including calcium, in vitro [55–58]. To directly demonstrate that primary cilium curving is caused by calcium binding to axonemal microtubules, we demonstrated that taxol attenuated the ability of calcium to cause primary cilium curving. This observation strongly supports our hypothesis that primary cilium curving is caused by calcium binding to the axonemal microtubule system.

4.2.3 Calcium is a common denominator between microtubule and primary cilium curving

Our data have shown that calcium may instigate curving of microtubules as well as primary cilia. However, the average curvature of primary cilia, under our experimental conditions, was an order of magnitude smaller than those of microtubules free in solution. If no other factors were involved that are capable of destabilizing the axonemal microtubule system, the

difference in extent of curvature could be due to the additional stabilization of the axonemal microtubule system by its intrinsic construction pattern conditions (nine doublets of interconnected microtubules). In spite of the apparent difference in the extent of curvature, it is likely that calcium is the common cause of the bending phenomena in both cilia and microtubules. Therefore, one can conclude that it is likely that curving of axonemal microtubules, due to calcium binding, allows curving of primary cilia under flow conditions.

4.3 Bifurcation in the extent of microtubule bending caused by calcium excess

The bifurcation phenomenon associated with microtubules bending caused by calcium is reflected in the appearance of the two different subpopulations of curved microtubules with distinctly different curvatures. It appears that the smaller curvature corresponds to the bending of the microtubule protofilament, formed by GDP-$\alpha\beta$-tubulin dimers, due to re-alignment between neighboring GDP-$\alpha\beta$-tubulin dimers: the bending amounts <24° [77]. In theory, this bending may be caused by a MAP-2 conformational change due to calcium binding to MAP-2. On the other hand, the bending with a larger curvature is likely to correspond to bending of the protofilament between α and β tubulin subunits: this bending amounts to <27° [77]. Similarly, this bending may be caused by conformational changes within MAP-2 that are associated with the relevant tubulin subunits. It is also possible that conformational changes within relevant tubulin subunits, caused by independent calcium binding to tubulin itself, can contribute to this bending. It is also possible that the two different curvatures may be produced by varying combinations of these two bending modalities.

It has been previously shown that microtubule-associated proteins (MAPs) make an important contribution in microtubule bending due to calcium binding [52]. Indeed, calcium binding "to either the low or high affinity Ca^{2+} binding sites on tubulin may decrease the interaction of $\alpha\beta$-tubulins with the microtubule-binding domain of MAPs, leading to an increase in curvature" [68]. In addition, microtubule stabilization by MAPs against calcium effects is very strong: "MAPs-free tubulin is nearly an order of magnitude more sensitive to Ca^{2+} than observed in the presence of MAPs" [78]. Therefore, the role of MAPs should be taken into account in microtubule bending caused by calcium. Our data show that irregularity in the MAP-2 super-lattice and detachment of MAP-2 accompanies microtubule regional curving.

4.4 Importance of non-linearities within the primary cilium intra-space in terms of calcium interactions with axonemal microtubules

Our data show that the bifurcation phenomenon is present in morphological changes of both, primary cilium and microtubules. The occurrence of bifurcations in turn strongly suggests that events related to the intra-cilium space are driven by non-linearities. Indeed, the first and foremost non-linearity relates to *'dynamic instability'* of microtubule growth. This non-linearity is underlined by the two other non-linearities, which involve strong and complex electrostatic interactions and cross diffusion. Both of these are strongly implicated by high level crowdedness within the intra-cilium space. The $\alpha\beta$-tubulin dimer, the intrinsic building block of microtubules, may undergo a great variety of conformational changes, which in turn instigate the non-equilibrium process known as *'dynamic instability'* [79, 80]. Dynamic instability consists of random inter-conversions between periods of fast shrinking and slow extension of a microtubule during its growth. Since its discovery, dynamic instability has become a hallmark of non-linear microtubule behavior [81].

Importantly, the primary cilium backbone, constituted by nine microtubule doublets known as axonemal microtubules (Fig. 1c), is directed toward the tip of the primary cilium, where the microtubule fast growing end, that exhibits prominent dynamic instability, is located. This indicates that there could be tight correlation between primary cilium morphological changes and axonemal microtubule dynamic instability. Therefore, it is reasonable to expect that diverse, rapid and reversible morphological changes of primary cilium are critically driven by non-linear characteristics of axonemal microtubule dynamic instability. In other words, the phenomenological similarity of non-linear dynamics of the primary cilium shortening/extension and in vitro microtubule shortening/extension may have a common molecular basis, which is the non-linearity of microtubule dynamic instability.

It is also important to note that the dynamic instability phenomenon may be additionally modulated by other strong nonlinearities, mediated by complex electrodynamic interactions and cross-diffusion that occur within the highly crowded primary cilium intra-space [69, 71, 82–86].

Electrodynamic conditioning originates from the strong surface charge of microtubules, including both the αβ-tubulin dimer and MAPs, as well as the bound calcium cationic charge. The surface of the αβ-tubulin dimer exhibits strong overall net negative charge density [87]. Apart from strong electrostatic forces, the overall net negative electric surface charge of the αβ-tubulin dimer generates a strong dipole moment pertained to each αβ-tubulin dimer [69, 88, 89]. Moreover, the existence of ionic clouds around individual microtubules has been quantitatively predicted, yielding non-linear ionic pulses along individual microtubules, and strong ionic coupling between them [69, 71, 82–85, 90, 91]. Furthermore, dipole moments can influence the dynamics of microtubule growth, by contributing to dynamic instability, by directly affecting the strength of αβ-tubulin dimer-dimer interactions [69, 88].

Additionally, these electrostatic forces may influence the way in which axonemal microtubules form and maintain their doublet structure, under the boundary conditions within the narrow and crowded intra-space of the primary cilium. The ionic clouds of individual microtubules and non-linear ionic pulses, in the case of nine doublets of radially organized microtubules within the primary cilium, may in turn generate a more complex electro-dynamic and integrative super-structure that includes all axonemal microtubules [88, 90]. The electro-dynamic phenomenon is of particular importance within the primary cilium, since the condensed ionic cloud may form an electrostatic mantle around the axonemal microtubules, all located within a small, closed, highly crowded space between the surface charge of axonemal microtubules and the charged primary cilium membrane.

Cross-diffusion of the calcium cation may be another source of non-linearity, since the movement of calcium through the primary cilium intra-space, its docking and final interaction with MAPs or the microtubule surface may all be affected by the electrostatic mantle. The axonemal set of nine microtubule doublets, including MAPs, occupies a substantial part of the intra-ciliary space (~70%). Apart from microtubule proteins, more than 1000 other protein species have been identified within the intra-ciliary space. Since the intra-ciliary space is defined by narrow boundary conditions, i.e., it is 200 nm in diameter and several microns in length, the intra-ciliary space seems highly crowded. Consequently, the high excluded volume determined by the high crowdedness is likely to significantly affect all interactions and freedom of motion of all particles, including proteins, and in particular small ions, such as the calcium cation. For example, assuming a high surface charge of the microtubule system and large excluded volume, cross-diffusion within the intra-cilium space is highly likely to essentially be a non-linear phenomenon [86]. Under conditions of cross-diffusion, the

concentration gradient of one species may change the gradient of another species. Therefore, the gradient of calcium cations may be influenced by the gradient of another species, and vice versa.

The motion of calcium cations within the intra-ciliary space may be modulated by both mechanochemical forces, such as cross-diffusion gradient forces, and electrodynamic forces. There may be strong coupling between these two non-linear phenomena within the intra-ciliary space. Consequently, our current data suggest that the interplay between these two forces may critically tune the calcium-dependent ability of microtubules to modulate signals, particularly electro-mechanical signals, orchestrated by microtubule morphological changes within the primary cilium [88].

Finally, the non-linear nature of the system is also highlighted by the minuscule amount of calcium cations necessary for bending of the primary cilium by means of microtubule skeleton bending. We have estimated that this critical amount is far smaller than the capacity of TRPP1/2 calcium channels by approximately a factor of 1.45×10^{11}. This amount of calcium is negligible, and would not be expected to significantly disturb the global level of cytosol calcium, but it is sufficient to instigate gross morphological changes with the primary cilium [3, 39, 66].

Speaking generally, instigation of gross changes within a system by a negligible amount of a certain agent is a typical characteristic of non-linear systems. The insight that our data provide into the non-liner nature of ciliary signaling highlights the potential importance of the small changes in calcium concentration being substantially multiplied in terms of ciliary functional characteristics. Microtubule dynamic instability, as a non-linear phenomenon, is endowed with substantial and sudden bifurcation points. Therefore, if the concentration of a certain agent, e.g., calcium, is slightly altered above or below the critical threshold, the microtubule system will undergo significant shortening/extending or bending/straightening. Therefore, under particular solution conditions, this effect may drive the whole system (primary cilium morphology) in one direction or the other. Consequently, non-linearity, together with the strong bifurcation points of axonemal microtubule dynamic instability, could be the starting point for understanding "dual and opposing roles of primary cilia in medullo-blastoma development" [15].

4.5 Conclusions

Calcium entry into primary cilia is regulated by calcium-sensitive polycystin channels (TRPP1/2). Our data strongly supports the hypothesis that calcium binding to axonemal microtubules in turn leads to nonlinear regulation of cilia morphology, in terms of curvature and length changes. This fundamental mechanism is highly likely to be of relevance in both health and disease, as the extracellular availability of calcium is tightly controlled, especially in the central nervous system.

Taken together, our work demonstrates that axonemal microtubules are not only tracks that merely support the transport of different proteins between the tip of primary cilia and their bases, but represent more complex, dynamic structures that are specifically sensitive to signaling agents, such as the second messenger calcium. This may explain the disassembly and re-assembly of primary cilia on coordinated time scales and in different phases of the cell cycle. Our results illustrate a few rather simple dynamic morphological changes of primary cilia in response to calcium binding. Moreover, it is reasonable to assume that complex dynamic responses of axonemal microtubules, which interact with signaling agents, play an

important role in the pathogenesis of various diseases. The development of future therapies for ciliopathies seems especially attractive in the context of cancer and nervous system aging.

Compliance with ethical standards

Conflict of interest   The authors declare that they have no conflicts of interest.

References

1. Satir, P., Christensen, S.T.: Overview of structure and function of mammalian cilia. Annu. Rev. Physiol. **69**, 377–400 (2007). https://doi.org/10.1146/annurev.physiol.69.040705.141236

2. Delling, M., DeCaen, P.G., Doerner, J.F., Febvay, S., Clapham, D.E.: Primary cilia are specialized calcium signalling organelles. Nature **504**(7479), 311–314 (2013). https://doi.org/10.1038/nature12833

3. DeCaen, P.G., Delling, M., Vien, T.N., Clapham, D.E.: Direct recording and molecular identification of the calcium channel of primary cilia. Nature **504**(7479), 315–318 (2013). https://doi.org/10.1038/nature12832

4. Nauli, S.M., Zhou, J.: Polycystins and mechanosensation in renal and nodal cilia. BioEssays **26**(8), 844–856 (2004). https://doi.org/10.1002/bies.20069

5. Toftgard, R.: Two sides to cilia in cancer. Nat. Med. **15**(9), 994–996 (2009). https://doi.org/10.1038/nm0909-994

6. Nauli, S.M., Jin, X., AbouAlaiwi, W.A., El-Jouni, W., Su, X., Zhou, J.: Non-motile primary cilia as fluid shear stress mechanosensors. Methods Enzymol. **525**, 1–20 (2013). https://doi.org/10.1016/B978-0-12-397944-5.00001-8

7. Davenport, J.R., Yoder, B.K.: An incredible decade for the primary cilium: a look at a once-forgotten organelle. Am. J. Physiol. Renal Physiol. **289**(6), F1159–F1169 (2005). https://doi.org/10.1152/ajprenal.00118.2005

8. Moorman, S.J., Ardon, Z., Shorr, A.Z.: The primary cilium as a gravitational force transducer and a regulator of transcriptional noise. Dev. Dynam. **237**, 1955–1959 (2008). https://doi.org/10.1002/dvdy.21493

9. Seeley, E.S., Nachury, M.V.: The perennial organelle: assembly and disassembly of the primary cilium. J. Cell Sci. **123**, 511–518 (2010). https://doi.org/10.1242/jcs.061093

10. Praetorius, H.A., Spring, K.R.: Removal of the MDCK cell primary cilium abolishes flow sensing. J. Membrane Biol. **191**, 69–76 (2002)

11. Salisbury, J.L.: Primary cilia: putting sensors together. Curr. Biol. **14**, R765–R767 (2004). https://doi.org/10.1016/j.cub.2004.09.016

12. Wheatley, D.N.: Primary cilia in normal and pathological tissues. Pathobiology **63**(4), 222–238 (1995)

13. Abdul-Majeed, S., Moloney, B.C., Nauli, S.M.: Mechanisms regulating cilia growth and cilia function in endothelial cells. Cell. Mol. Life Sci. **69**(1), 165–173 (2012). https://doi.org/10.1007/s00018-011-0744-0

14. Abdul-Majeed, S., Nauli, S.M.: Dopamine receptor type 5 in the primary cilia has dual chemo- and mechano-sensory roles. Hypertension **58**(2), 325–331 (2011). https://doi.org/10.1161/hypertensionaha.111.172080

15. Abou Alaiwi, W.A., Lo, S.T., Nauli, S.M.: Primary cilia: highly sophisticated biological sensors. Sensors (Basel) **9**(9), 7003–7020 (2009). https://doi.org/10.3390/s90907003

16. Nauli, S.M., Alenghat, F.J., Luo, Y., Williams, E., Vassilev, P., Li, X., Elia, A.E., Lu, W., Brown, E.M., Quinn, S.J., Ingber, D.E., Zhou, J.: Polycystins 1 and 2 mediate mechanosensation in the primary cilium of kidney cells. Nat. Genet. **33**(2), 129–137 (2003). https://doi.org/10.1038/ng1076

17. Pazour, G.J., Witman, G.B.: The vertebrate primary cilium is a sensory organelle. Curr. Opin. Cell Biol. **15**(1), 105–110 (2003)

18. Scholey, J.M., Anderson, K.V.: Intraflagellar transport and cilium-based signaling. Cell **125**(3), 439–442 (2006). https://doi.org/10.1016/j.cell.2006.04.013

19. Shah, J.V.: Cells in tight spaces: the role of cell shape in cell function. J. Cell Biol. **191**(2), 233–236 (2010). https://doi.org/10.1083/jcb.201009048

20. Pitaval, A., Tseng, Q., Bornens, M., Thery, M.: Cell shape and contractility regulate ciliogenesis in cell cycle-arrested cells. J. Cell Biol. **191**(2), 303–312 (2010). https://doi.org/10.1083/jcb.201004003

21. Goto, H., Inoko, A., Inagaki, M.: Cell cycle progression by the repression of primary cilia formation in proliferating cells. Cell. Mol. Life Sci. **70**(20), 3893–3905 (2013). https://doi.org/10.1007/s00018-013-1302-8

22. Tucker, R.W., Pardee, A.B., Fujiwara, K.: Centriole ciliation is related to quiescence and DNA synthesis in 3T3 cells. Cell **17**(3), 527–535 (1979)

23. Plotnikova, O.V., Golemis, E.A., Pugacheva, E.N.: Cell cycle-dependent ciliogenesis and cancer. Cancer Res. **68**(7), 2058–2061 (2008). https://doi.org/10.1158/0008-5472.CAN-07-5838

24. Fry, A.M., Leaper, M.J., Bayliss, R.: The primary cilium: guardian of organ development and homeostasis. Organ **10**(1), 62–68 (2014). https://doi.org/10.4161/org.28910

25. Gerdes, J.M., Davis, E.E., Katsanis, N.: The vertebrate primary cilium in development, homeostasis, and disease. Cell **137**(1), 32–45 (2009). https://doi.org/10.1016/j.cell.2009.03.023

26. Oishi, I., Kawakami, Y., Raya, A., Callol-Massot, C., Izpisua Belmonte, J.C.: Regulation of primary cilia formation and left-right patterning in zebrafish by a noncanonical Wnt signaling mediator, duboraya. Nat. Genet. **38**(11), 1316–1322 (2006). https://doi.org/10.1038/ng1892

27. Moser, J.J., Fritzler, M.J., Rattner, J.B.: Ultrastructural characterization of primary cilia in pathologically characterized human glioblastoma multiforme (GBM) tumors. BMC Clin. Pathol. **14**, 40 (2014). https://doi.org/10.1186/1472-6890-14-40

28. Hassounah, N.B., Nagle, R., Saboda, K., Roe, D.J., Dalkin, B.L., McDermott, K.M.: Primary cilia are lost in preinvasive and invasive prostate cancer. PLoS ONE **8**(7), e68521 (2013). https://doi.org/10.1371/journal.pone.0068521

29. Yuan, K., Frolova, N., Xie, Y., Wang, D., Cook, L., Kwon, Y.J., Steg, A.D., Serra, R., Frost, A.R.: Primary cilia are decreased in breast cancer: analysis of a collection of human breast cancer cell lines and tissues. J. Histochem. Cytochem. **58**(10), 857–870 (2010). https://doi.org/10.1369/jhc.2010.955856

30. Christensen, S.T., Pedersen, L.B., Schneider, L., Satir, P.: Sensory cilia and integration of signal transduction in human health and disease. Traffic **8**(2), 97–109 (2007). https://doi.org/10.1111/j.1600-0854.2006.00516.x

31. Badano, J.L., Mitsuma, N., Beales, P.L., Katsanis, N.: The ciliopathies: an emerging class of human genetic disorders. Annu. Rev. Genomics Hum. Genet. **7**, 125–148 (2006). https://doi.org/10.1146/annurev.genom.7.080505.115610

32. Prasad, R.M., Jin, X., Nauli, S.M.: Sensing a sensor: identifying the mechanosensory function of primary cilia. Biosensors (Basel) **4**(1), 47–62 (2014). https://doi.org/10.3390/bios4010047

33. Jin, X., Mohieldin, A.M., Muntean, B.S., Green, J.A., Shah, J.V., Mykytyn, K., Nauli, S.M.: Cilioplasm is a cellular compartment for calcium signaling in response to mechanical and chemical stimuli. Cell. Mol. Life Sci. **71**(11), 2165–2178 (2014). https://doi.org/10.1007/s00018-013-1483-1

34. Ishihara, Y., Sugawara, Y., Kamioka, H., Kawanabe, N., Hayano, S., Balam, T.A., Naruse, K., Yamashiro, T.: *Ex vivo* real-time observation of Ca^{2+} signaling in living bone in response to shear stress applied on the bone surface. Bone **53**(1), 204–215 (2013). https://doi.org/10.1016/j.bone.2012.12.002

35. Praetorius, H.A., Spring, K.R.: Bending the MDCK cell primary cilium increases intracellular calcium. J. Membr. Biol. **184**, 71–79 (2001)

36. Grantham, J.J.: Clinical practice. Autosomal dominant polycystic kidney disease. N. Engl. J. Med. **359**(14), 1477–1485 (2008). https://doi.org/10.1056/NEJMcp0804458

37. Torres, V.E., Harris, P.C., Pirson, Y.: Autosomal dominant polycystic kidney disease. Lancet **369**, 1287–1300 (2007). https://doi.org/10.1016/S0140-6736(07)60601-1

38. Bichet, D., Peters, D., Patel, A.J., Delmas, P., Honore, E.: Cardiovascular polycystins: insights from autosomal dominant polycystic kidney disease and transgenic animal models. Trends Cardiovasc. Med. **16**(8), 292–298 (2006). https://doi.org/10.1016/j.tcm.2006.07.002

39. Patel, A., Honoré, E.: Polycystins and renovascular mechanosensory transduction. Nat. Rev. Nephrol. **6**, 530–538 (2010). https://doi.org/10.1038/nrneph.2010.97

40. Montalbetti, N., Li, Q., Wu, Y., Chen, X.Z., Cantiello, H.F.: Polycystin-2 cation channel function in the human syncytiotrophoblast is regulated by microtubular structures. J. Physiol. **579**(Pt 3), 717–728 (2007). https://doi.org/10.1113/jphysiol.2006.125583

41. Scemes, E., Suadicani, S.O., Spray, D.C.: Intercellular communication in spinal cord astrocytes: fine tuning between gap junctions and P2 nucleotide receptors in calcium wave propagation. J. Neurosci. **20**(4), 1435–1445 (2000)

42. Cole, R., De Vellis, J.: Astrocyte and oligodendrocyte cultures. In: Fedoroff, S.S., Richardson, A. (eds.) Protocols for Neural Cell Cultures Pp. 117–130. Humana Press, New Jersey (1997)

43. Wiesinger, H., Schuricht, B., Hamprecht, B.: Replacement of glucose by sorbitol in growth medium causes selection of astroglial cells from heterogeneous primary cultures derived from newborn mouse brain. Brain Res. **550**(1), 69–76 (1991)

44. Bennett, M.R., Buljan, V., Farnell, L., Gibson, W.G.: Purinergic junctional transmission and propagation of calcium waves in spinal cord astrocyte networks. Biophys. J. **91**(9), 3560–3571 (2006). https://doi.org/10.1529/biophysj.106.082073

45. Bennett, M.R., Buljan, V., Farnell, L., Gibson, W.G.: Purinergic junctional transmission and propagation of calcium waves in cultured spinal cord microglial networks. Purinergic Signal. **4**(1), 47–59 (2008). https://doi.org/10.1007/s11302-007-9076-9

46. Takano, H., Sul, J.Y., Mazzanti, M.L., Doyle, R.T., Haydon, P.G., Porter, M.D.: Micropatterned substrates: approach to probing intercellular communication pathways. Anal. Chem. **74**(18), 4640–4646 (2002)

47. Recknor, J.B., Recknor, J.C., Sakaguchi, D.S., Mallapragada, S.K.: Oriented astroglial cell growth on micropatterned polystyrene substrates. Biomaterials **25**, 2753–2767 (2004). https://doi.org/10.1016/j.biomaterials.2003.11.045

48. Whitesides, G.M., Ostuni, E., Takayama, S., Jiang, X., Ingber, D.E.: Soft lithography in biology and biochemistry. Annu. Rev. Biomed. Eng. **3**, 335–373 (2001). https://doi.org/10.1146/annurev.bioeng.3.1.335

49. Ott, C., Lippincott-Schwartz, J.: Visualization of live primary cilia dynamics using fluorescence microscopy. Curr. Protoc. Cell Biol. **Unit 4**(26), 1–22 (2012). https://doi.org/10.1002/0471143030.cb0426s57

50. Shelanski, M.L., Gaskin, F., Cantor, C.R.: Microtubule assembly in the absence of added nucleotides. Proc. Natl. Acad. Sci. U. S. A. **70**(3), 765–768 (1973)

51. Kim, H., Binder, L.I., Rosenbaum, J.L.: The periodic association of MAP-2 with brain microtubules *in vitro*. J. Cell Biol. **80**(2), 266–276 (1979)

52. Buljan, V., Ivanova, E.P., Cullen, K.M.: How calcium controls microtubule anisotropic phase formation in the presence of microtubule-associated proteins *in vitro*. Biochem. Biophys. Res. Commun. **381**(2), 224–228 (2009). https://doi.org/10.1016/j.bbrc.2009.02.028

53. Langford, G.M.: Length and appearance of projections on neuronal microtubules *in vitro* after negative staining: evidence against a crosslinking function for MAPs. J. Ultrastruct. Res. **85**(1), 1–10 (1983)

54. Karr, T.L., Kristofferson, D., Purich, D.L.: Calcium ion induces endwise depolymerization of bovine brain microtubules. J. Biol. Chem. **255**(24), 11853–11856 (1980)

55. Schiff, P.B., Fant, J., Horwitz, S.B.: Promotion of microtubule assembly *in vitro* by taxol. Nature **277**(5698), 665–667 (1979)

56. Arnal, I., Wade, R.H.: How does taxol stabilize microtubules? Curr. Biol. **5**(8), 900–908 (1995)

57. Vater, W., Bohm, K.J., Unger, E.: Tubulin assembly in the presence of calcium ions and taxol: microtubule bundling and formation of macrotubule-ring complexes. Cell Motil. Cytoskeleton **36**(1), 76–83 (1997). https://doi.org/10.1002/(SICI)1097-0169(1997)36:1<76::AID-CM7>3.0.CO;2-F

58. Amos, L.A., Lowe, J.: How taxol stabilises microtubule structure. Chem. Biol. **6**(3), R65–R69 (1999)

59. Kern, W.F., Bland, J.R.: "Theorem of Pappus." Solid Mensuration with Proofs, vol. 2. Wiley, New York (1948)

60. Fong, K.C., Babitch, J.A., Anthony, F.A.: Calcium binding to tubulin. Biochim. Biophys. Acta **952**, 13–19 (1988)

61. Solomon, F.: Binding sites for calcium on tubulin. Biochemistry **16**(3), 358–363 (1977)

62. Serrano, L., Valencia, A., Caballero, R., Avila, J.: Localization of the high affinity calcium-binding site on tubulin molecule. J. Biol. Chem. **261**(15), 7076–7081 (1986)

63. Sui, H., Downing, K.H.: Molecular architecture of axonemal microtubule doublets revealed by cryo-electron tomography. Nature **442**(7101), 475–478 (2006). https://doi.org/10.1038/nature04816

64. Hernandez, M.A., Serrano, L., Avila, J.: Microtubule-associated protein, MAP2, is a calcium-binding protein. Biochim. Biophys. Acta **965**(2–3), 195–201 (1988)

65. Vassilev, P.M., Guo, L., Chen, X.-Z., Segal, Y., Peng, J.-B., Basora, N., Babakhanlou, H., Cruger, G., Kanazirska, M., Ye, C.-P., Brown, E.M., Hediger, M.A., Zhou, J.: Polycystin-2 is a novel cation channel implicated in defective intracellular Ca^{2+} homeostasis in polycystic kidney disease. Biochem. Biophys. Res. Commun. **282**, 341–350 (2001)

66. Cantero, M.R., Cantiello, H.F.: Calcium transport and local pool regulate polycystin-2 (TRPP2) function in human syncytiotrophoblast. Biophys. J. **15**, 365–375 (2013). https://doi.org/10.1016/j.bpj.2013.05.058

67. Lobert, S., Hennington, B.S., Correia, J.J.: Multiple sites for subtilisin cleavage of tubulin: effects of divalent cations. Cell Motil. Cytoskeleton **25**(3), 282–297 (1993). https://doi.org/10.1002/cm.970250308

68. Ferralli, J., Doll, T., Matus, A.: Sequence analysis of MAP2 function in living cells. J. Cell Sci. **107**(Pt 11), 3115–3125 (1994)

69. Tuszynski, J.A., Brown, J.A., Crawford, E., Carpenter, E.J., Nip, M.L.A., Dixon, J.M., Sataric, M.V.: Molecular dynamics simulations of tubulin structure and calculations of electrostatic properties of microtubules. Math. Comput. Model. **41**, 1055–1070 (2005). https://doi.org/10.1016/j.mcm.2005.05.002

70. Lefèvre, J., Chernov, K.G., Joshi, V., Delga, S., Toma, F., Pastrè, D., Curmi, P.A., Savarin, P.: The C-terminus of tubulin, a versatile partner for cationic molecules. J. Biol. Chem. **286**(4), 3065–3078 (2011). https://doi.org/10.1074/jbc.M110.144089

71. Priel, A., Ramos, A.J., Tuszynski, J.A., Cantiello, H.F.: Effect of calcium on electrical energy transfer by microtubules. J. Biol. Phys. **34**, 475–485 (2008). https://doi.org/10.1007/s10867-008-9106-z

72. Siwy, Z.S., Powell, M.R., Petrov, A., Kalman, E., Trautmann, C., Eisenberg, R.S.: Calcium-induced voltage gating in single conical nanopores. Nano Lett. **6**(8), 1729–1734 (2006). https://doi.org/10.1021/nl061114x

73. Sataric, M.V., Sekulic, D., Živanov, M.: Solitonic ionic currents along microtubules. J. Comput. Theor. Nanosci. **7**, 1–10 (2010). https://doi.org/10.1166/jctn.2010.1609

74. Li, H., DeRosier, D.J., Nicholson, W.V., Nogales, E., Downing, K.H.: Microtubule structure at 8Å resolution. Structure **10**, 1317–1328 (2002)

75. Tagliazucchi, M., Szleifer, I.: Transport mechanisms in nanopores and nanochannels: can we mimic nature? Mater. Today **18**(3), 131–142 (2015). https://doi.org/10.1016/j.mattod.2014.10.020

76. Ma, L., Cockroft, S.L.: Biological nanopores for single-molecule biophysics. Chembiochem **11**(1), 25–34 (2010). https://doi.org/10.1002/cbic.200900526

77. Melki, R., Carlier, M.F., Pantaloni, D., Timasheff, S.N.: Cold depolymerization of microtubules to double rings: geometric stabilization of assemblies. Biochemistry **28**(23), 9143–9152 (1989)

78. Berkowitz, S.A., Wolff, J.: Intrinsic calcium sensitivity of tubulin polymerization. The contributions of temperature, tubulin concentration, and associated proteins. J. Biol. Chem. **256**(21), 11216–11223 (1981)

79. Brouhard, G.J., Rice, L.M.: The contribution of αβ-tubulin curvature to microtubule dynamics. J. Cell Biol. **207**(3), 323–334 (2014). https://doi.org/10.1083/jcb.201407095

80. Mitchison, T., Kirschner, M.: Dynamic instability of microtubule growth. Nature **312**(5991), 237–242 (1984)

81. Kirschner, M., Mitchison, T.: Beyond self-assembly: from microtubules to morphogenesis. Cell **45**(3), 329–342 (1986)

82. Tuszynski, J.A., Hameroff, S., Sataric, M.V., Trpisova, B., Nip, M.L.A.: Ferroelectric behavior in microtubule dipole lattices - implications for information-processing, signaling and assembly disassembly. J. Theor. Biol. **174**, 371–380 (1995)

83. Tuszynski, J.A., Brown, J.A., Hawrylak, P.: Dielectric polarization, electrical conduction, information processing and quantum computation in microtubules. Are they plausible? Phil. Trans. R. Soc. Lond. A **356**, 1897–1926 (1998)

84. Tuszynski, J.A., Portet, S., Dixon, J.M., Luxford, C., Cantiello, H.F.: Ionic wave propagation along actin filaments. Biophys. J. **86**, 1890–1903 (2004). https://doi.org/10.1016/S0006-3495(04)74255-1

85. Sekulić, D.L., Satarić, B.M., Tuszynski, J.A., Satarić, M.V.: Nonlinear ionic pulses along microtubules. Eur. Phys. J. E. Soft Matter **34**, 49 (2011). https://doi.org/10.1140/epje/i2011-11049-0

86. Vanag, V.K., Epstein, I.R.: Pattern formation mechanisms in reaction-diffusion systems. Int. J. Dev. Biol. **53**, 673–681 (2009). https://doi.org/10.1387/ijdb.072484vv

87. Minoura, I., Muto, E.: Dielectric measurement of individual microtubules using the electroorientation method. Biophys. J. **90**(10), 3739–3748 (2006). https://doi.org/10.1529/biophysj.105.071324

88. Priel, A., Tuszynski, J.A., Cantiello, H.F.: The dendritic cytoskeleton as a computational device: an hypothesis. In: Tuszynski, J.A. (ed.) The Emerging Physics of Consciousness. pp. 293–325. Springer, (2006)

89. Brown, J.A., Tuszynski, J.A.: The possible relationship between cell shape and electric fields. J. Theor. Biol. **200**(2), 245–247 (1999). https://doi.org/10.1006/jtbi.1999.0984

90. Sataric, M.V., Ilić, D.I., Ralević, N., Tuszynski, J.A.: A nonlinear model of ionic wave propagation along microtubules. Eur. Biophys. J. **38**, 637–647 (2009). https://doi.org/10.1007/s00249-009-0421-5

91. Sataric, M.V., Sataric, B.M.: Ionic pulses along cytoskeletal protofilaments. J. Physics: Conf. Ser. **329**, 012009 (2011). https://doi.org/10.1088/1742-6596/329/1/012009

92. Dye, R.B., Fink, S.P., Williams, R.C.J.: Taxol-induced flexibility of microtubules and its reversal by MAP-2 and tau. J. Biol. Chem. **268**(10), 6847–6850 (1993)

93. Felgner, H., Frank, R., Biernat, J., Mandelkow, E.M., Mandelkow, E., Ludin, B., Matus, A., Schliwa, M.: Domains of neuronal microtubule-associated proteins and flexural rigidity of microtubules. J. Cell Biol. **138**(5), 1067–1075 (1997)

94. Kim, H., Jensen, C.G., Rebhun, L.I.: The binding of MAP-2 and tau on brain microtubules *in vitro*: implications for microtubule structure. Ann. N. Y. Acad. Sci. **466**, 218–239 (1986)